Biomedical Microdevices (2019) 21: 89
https://doi.org/10.1007/s10544-019-0437-2

Preparation of BMP-2/chitosan/hydroxyapatite antibacterial bio-composite coatings on titanium surfaces for bone tissue engineering

Xiaolin Wang [1] · Baoe Li [1] · Ce Zhang [1]

Published online: 26 October 2019
© Springer Science+Business Media, LLC, part of Springer Nature 2019

Abstract
In this paper, petaling hydroxyapatite (HA)/TiO_2 composite coatings were firstly prepared on titanium (Ti) surface by one-step micro-arc oxidation (MAO), and then pure chitosan (CS) and bone morphogenic protein-2 (BMP-2)-encapsulated CS coatings were respectively loaded on the HA/TiO_2 surfaces by dip-coating method to endow Ti with good antibacterial and biological properties. The bonding strength between coatings was studied by scratch method. The degradability of CS, BMP-2 release behavior, bioactivity, biocompatibility and antibacterial activity of the obtained (BMP-2)/CS/HA/TiO_2 coatings were examined by *in vitro* tests. The results showed that, the thicker the HA layer, the larger the loaded BMP-2 and CS amount, resulting in better bonding strength between coatings, antibacterial activity and biocompatibility. In addition, with the increase of CS concentration, more CS was loaded on HA coatings, which benefited the increase of CS degrading amount, the prolonged CS degradation time and BMP-2 release time, resulting in improved antibacterial and biological property. All CS/HA/TiO_2 coatings accelerated cell adhesion, spreading and proliferation, and promoted HA formation in simulated body fluids (SBF). After loading BMP-2 in CS, the BMP-2 can significantly improve cell adhesion, spreading and proliferation, and the loaded amount can also be controlled by the concentration of BMP-2 solution. The present study indicates that, by controlling the thickness of HA layers and concentrations of CS and BMP-2 solutions, the Ti implant material with excellent biological and antibacterial properties can be achieved.

Keywords Hydroxyapatite · Chitosan · BMP-2 · Antibacterial activity · Biological property

1 Introduction

Titanium (Ti) is one of the most widely used implant materials for bone repair because of its excellent mechanical property, chemical stability and biocompatibility (Arifin et al. 2014; Han et al. 2017). But Ti-based implant was bioinnert and cannot bone-bond with bone tissues, which hindered the application of this material. To improve the biological properties of Ti implant and achieve firm combination with bone tissues, hydroxyapatete (HA) is frequently deposited on Ti surface due to that HA is the main inorganic component of the natural bone tissues. Among the many methods of preparing HA coatings on metal surface, micro-arc oxidation (MAO) is a convenient, effective and economical technique. By MAO, HA/TiO_2 composite ceramic coatings can be prepared rapidly on Ti surfaces and the binding force between HA coatings and Ti substrates can be improved due to the existence of the rough interfacial layer of TiO_2 (Wang et al. 2018). Yet, the HA/TiO_2 coatings are lacking in antibacterial activity, which is a serious problem that can lead to postoperative infection and even surgical failure. Therefore, it is necessary to modify the HA-coated implants to have good antibacterial property. Based on the literature, antibacterial materials can be introduced to the implant surfaces to lower the risk of postoperative infection by preventing the bacterial adhesion and proliferation. Compared with other antibacterial materials, chitosan (CS) has more advantages due to its suitable nontoxicity, biocompatibility and degradation (He et al. 2017). Some researchers also explored the combination of HA and CS to achieve good biological and antibacterial property (Yu et al.

Electronic supplementary material The online version of this article (https://doi.org/10.1007/s10544-019-0437-2) contains supplementary material, which is available to authorized users.

✉ Xiaolin Wang
176050716@qq.com

✉ Baoe Li
libaoe@hotmail.com

[1] School of Materials Science and Engineering, Hebei University of Technology, No.1 Dingzigu Road, Hongqiao District, Tianjin, China

2018a, b; Zhang et al. 2017). And their results showed that, although the antibacterial property was enhanced, its biological property was still not satisfying. For serious diseases that requires rapid wound healing, it can hardly meet the clinical needs. To strengthen the biological property of bio-composite coatings, bone morphogenic protein-2 (BMP-2), which is one of the most widely used growth factors because of its essential role in bone regeneration, has been usually used in biological implantation. But BMP-2 exhibits short-range diffusion and acts locally due to its short half-lives and slow diffusion, resulting in that BMP-2 must be carried and released in a controlled and sustained manner. It has been reported that biodegradable polymer materials could be an excellent carrier for growth factors (Hsieh et al. 2017; Skodje et al. 2015), therefore, CS may be a suitable carrier for BMP-2 due to its degradable and biocompatible properties (Yun 2013). After implantation, CS would control the release rate of BMP-2 by adjusting the degradation rate. Although there have been some reports of the HA/CS/BMP-2 microspheres or scaffolds to accelerate bone healing (Sun et al. 2018; Liu et al. 2013; He et al. 2014; Wang et al. 2014), those implants often have poor mechanical properties, especially for load-bearing bone tissues. Up to now, there has been no reports of preparing BMP-2/CS/HA/TiO_2 coatings on Ti surfaces. On the other hand, after implanted in organisms, the adhesion strength directly affects the long-term stability of the implant, and the fast peeling of effective coatings from substrates means the failure of the expected good effects. It has been reported that the coating adhesion strength is controlled by the the properties of the coatings and substrates, such as fracture strength, hardness, microstructure, modulus of elasticity, composition and thickness and the test parameters (Sharifi et al. 2018). Thus, for the prepared BMP-2/CS/HA coatings, there is necessary to study the adhesion strength of the prepared composite coatings on Ti substrates.

In this work, HA/TiO_2 coatings with different thickness were firstly prepared on Ti surfaces by MAO technology, and then pure CS and BMP-2 encapsulated CS with various concentrations were loaded on the HA/TiO_2 surfaces. It was expected that the stability, biological properties and antibacterial activity of the Ti surface would be significantly improved by the BMP-2/CS/HA/TiO_2 coating, and the research results can be a guidance for the surface modification of Ti-based implant material. The loaded CS amount, degrading rate and the release behavior of the BMP-2 from different BMP-2/CS/HA/TiO_2 coatings were investigated and compared. The biological properties were evaluated by simulated body fluids (SBF) soaking test and MC3T3-E1 cell co-culture experiment. The antibacterial effect against *E. coli* was evaluated by the optical technique and bacterial counting method.

2 Experimental methods

2.1 Materials preparation

Commercially pure Ti plates (TA1, Tianjin, China) with the diameter of 10 mm and the thickness of 1 mm were firstly polished with abrasive paper (800#, 1000#, 1500# and 2000#), washed with de-ionized water, and then used as the substrates for MAO treatment to obtain HA/TiO_2 composite coatings on Ti surfaces. The electrolytes were prepared by dissolving analytically pure $(CH_3COO)_2Ca{\cdot}H_2O$ and $NaH_2PO_4{\cdot}2H_2O$ in de-ionized water with concentrations of 0.2 mol/l and 0.1 mol/l respectively. The voltage - current - time, frequency and duty ratio were separately set at 400 V-0.2 A - 3 min (MAO-1), 360 V - 0.4 A - 5 min (MAO-2), and 360 V - 0.5 A - 8 min (MAO-3), 100 HZ and 50%. During MAO process, Ti was used as anode, platinum plate was cathode, and the distance between the two electrodes was 5 cm. To prepare the pure CS-coated HA/TiO_2 (CS/HA/TiO_2) and the BMP-2-encapsulated CS-coated HA/TiO_2 (BMP-2/CS/HA/TiO_2), the as-obtained HA/TiO_2 coatings were dipped in 3 ml of the following solutions for 3 min and then lifted out in a rate of 150 mm/min. The applied solutions were as follows: (a) CS solutions (0.5, 1, 3 and 4 mg/ml) which were prepared by dissolving pure CS in 2 vol% glacial acetic acid; (b) BMP-2 solutions (3.4, 6.8 and 10 μg/ml) which were diluted from a BMP-2 stock solution with phosphate buffer solution (PBS) and the BMP-2 stock solution was prepared by dissolving BMP-2 in 2 vol% glacial acetic acid (10 μg/ml); (c) BMP-2/CS solutions which were prepared by mixing 50 μl of BMP-2 solution with 2, 950 μl of sterile-filtered CS solution. The specimens were allowed to dry in an oven at 60 °C for 24 h and preserved in sterile conditions. The parameters used to prepare the different composite coatings were showed in Table 1.

2.2 Surface characterization

The surface morphology and cross-sections of the specimens were examined by scanning electron microscopy (SEM, Hitachi S-4800) and the energy dispersive X-ray analyzer (EDS)_was used for elemental analysis. The XRD patterns of the specimens were obtained at room temperature using an analytical XPERTPRO powder diffractometer (Cu Kα radiation) operating at a voltage of 40 KV. A few micrograms of the obtained coating surfaces were scraped off and mixed with KBr, then pressed for structural analysis using fourier transferinfrared (FTIR) spectroscopy. The loaded CS amount was studied by weighing method. The adhesive force was tested by a WS-92 scratch tester. The loading rate was 50 N/min with the final load of 50 N. Rough-meter (TIME 3200, Tianjin, China) was used to obtain surface roughness. Static contact angles (CAs, OCA30) were measured with the

Table 1 Parameters used to prepare the composite coatings with different CS and BMP-2 amounts

Sample	Concentration of CS (mg/ml)	Concentration of BMP-2 (ng/3 ml)
1CS/MAO-1	1	–
3BMP-2/1CS/MAO-1	1	500
1CS/MAO-2	1	–
3BMP-2/1CS/MAO-2	1	500
1CS/MAO-3	1	–
3BMP-2/1CS/MAO-3	1	500
1BMP-2/1CS/MAO-3	1	170
2BMP-2/1CS/MAO-3	1	340
0.5CS/MAO-3	0.5	–
3BMP-2/0.5CS/MAO-3	0.5	500
3CS/MAO-3	3	–
3BMP-2/3CS/MAO-3	3	500
4CS/MAO-3	4	–
3BMP-2/4CS/MAO-3	4	500

deionized water at room temperature to evaluate the surface hydrophilicity.

2.3 Degradation of the CS containing composite coatings

There were 8 samples for one group and 3 groups were weighted for each kind of CS/HA/TiO_2 coating, to calculate the CS degradation rate. The degradation of the biocomposites was studied by soaking in PBS - lysozyme solution whose concentration was 0.025 mg/ml (similar to human serum (Peng et al. 2014). The samples were kept in the solutions at 37 °C for various time periods up to 4 weeks. Per 2 or 3 days the PBS - lysozyme solution was replaced by fresh solution. At the end of each time point, the samples were taken out, rinsed with distilled water, and vacuum dried at 60 °C to constant weight, and then the degradation was characterized by SEM images and weight loss. In addition, to observe the surface morphology after CS degradation, the composite coating was also soaked in the 0.500 mg/ml PBS - lysozyme solution, and the high concentration was used to accelerate the CS degradation process and shorten the experiment period.

2.4 *In vitro* BMP-2 release study

To evaluate the release rate of BMP-2 on different BMP-2/CS/HA/TiO_2 composite coatings, 3 samples of each group were separately incubated in 5 ml of PBS - lysozyme (0.025 mg/ml) solutions at 37 °C. The concentration of the solution was similar to that in human serum (0.020 ± 0.003 mg/ml) (Peng et al. 2014). At the time intervals of 4, 8, 12, 18, 24 and 30 days, the solutions were collected and replaced with fresh ones. The concentrations of BMP-2 in the collected extractions were determined using mouse BMP-2 ELISA kit (EK0311, Boster, China). The total amount of BMP-2 released over a certain period and the total loaded amount were accumulated, and normalized with respect to the total protein content.

2.5 Antibacterial activity evaluation

The antibacterial activity of the samples was evaluated by the bacterial counting method and optical technique. The microorganism of *E. coli* was used during the evaluation since it is one of the major causes of all infections. The samples were sterilized by ultraviolet radiation lamp of 100 W for 8 h before experiments. Each group of the samples with total coating area of 5.4 cm^2 were immersed in 20 ml nutrient solution containing *E. coli* at a concentration of ~10^8 CFU/ml and incubated at 37 °C for 24 h (40 rpm). After that, 50 μl sonicated solution was diluted 10^6 times by pure nutrient culture solution. Then 100 μl diluted solution was inoculated onto a standard agar culture medium. After incubation at 37 °C for 24 h, the active bacteria were counted. While for the optical technique, the samples were incubated in bacteria suspension for 40 h (each group of the samples with total coating area of 2.4 cm^2), and then the viable bacteria in the suspension was evaluated by ultraviolet spectrophotometry.

2.6 Bioactivity evaluation

Bioactivity of different BMP-2/CS/HA/TiO_2 composite coatings was evaluated by investigating their influence on bone-like apatite formation after soaking in a 1.5 SBF solution. A standard 1.5 SBF solution consisted of the following analysis grade chemical reagents in deionized water: 9.8206 g/l NaCl, 3.4020 g/l $NaHCO_3$, 0.5596 g/l KCl, 0.4020 g/l $Na_2HPO_4 \cdot 7H_2O$, 0.4576 g/l $MgCl_2 \cdot 6H_2O$, 0.5520 g/l $CaCl_2 \cdot 2H_2O$, 0.1066 g/l Na_2SO_4, and 9.0856 g/l Tris. The pH of 1.5 SBF solutions was adjusted to 7.4. Each sample of HA/TiO_2 and BMP-2/CS/HA/TiO_2 composite coatings was respectively immersed in 10 ml 1.5 SBF solutions at 37 °C for 12 days, with refreshing per 2 days.

2.7 Biocompatibility evaluation

The mouse osteoblastic cell line MC3T3-E1 was purchased from Cell Resource Center (IBMS, CAMS/PUMC, China). The cells were seeded on the coating surfaces at a density of 7×10^4 cells/cm^2, and then cultured in alpha minimal essential medium (α-MEM) supplemented with 10% FBS and 1% penicillin-streptomycin at 37 °C with 5% CO_2 as the humidifying air. After cultured for 1 and 4 days, the cell viability and proliferation were determined utilizing Cell Counting Kit-8

(CCK-8, Dojindo, Kumamoto, Japan) according to the protocol.

The cells were also fixed with 2.5% glutaraldehyde (Nanjing institute of biological engineering, China) at 4 °C for 12 h, and then dehydrated by successive immersion in 40%, 50%, 60%, 70%, 75%, 80%, 85%, 90%, 95% and 100% ethanol each for 15 min and each gradient dehydrated twice. The cells were finally dried in hexamethyl-disilazane (HMDS) for 15 min, and observed by SEM.

2.8 Statistical analysis

Experiments were run in triplicate per sample. Standard deviations were plotted as error bars for the data points on all figures. Statistically significant differences were assessed by SAS. Difference with p values ≤0.05 was considered to be significant.

3 Results and discussion

3.1 Physicochemical characterizations

Figure 1a showed the XRD spectra of different specimens. It can be seen that after MAO treatment, TiO_2 and HA were formed on Ti surface, illustrating successful synthesis of the HA/TiO_2 composite coatings. For all BMP-2/CS loaded MAO surfaces, there were also the peaks of CS at around 11.5° and 21° (Lowe et al. 2016; Mohamed et al. 2017), suggesting that CS was successfully loaded on HA/TiO_2 surfaces by dip-coating method. With the increase of CS concentration, the intensity of CS peaks became stronger, indicating that, the larger the CS concentration, the more CS loaded on surface. CS peak at 21° did not appear in spectrum of 3BMP-2/1CS/MAO-1 but showed in spectrum of 3BMP-2/1CS/MAO-3, meaning that the HA layer has effect on CS amount loaded on the surface. However, the peaks of HA at around 32° became weak, which may be due to the varying degrees of the coverage of BMP-2/CS on HA coatings (observed in Fig. 2). There were no obvious peaks representing BMP-2 in all of the spectra, because the quantity is too small to be detected.

Figure 1b was the FTIR spectra of different surface coatings. The peaks standing for PO_4^{3-}, HPO_4^{2-} and -OH were observed in BMP-2/CS/HA/TiO_2 and HA/TiO_2 surfaces, confirming the existence of HA on surfaces. That element C existing in the HA/TiO_2 coatings is due to the replace of PO_4^{3-} by CO_3^{2-} from CO_2 atmosphere during MAO treatment, which is in good accordance with the literature (Li et al. 2017). For different BMP-2/CS/HA/TiO_2 surfaces, there were also no characteristic peaks representing BMP-2 because the content of BMP-2 on surfaces was too trace to be detected. However, -CH_2 group that was one of the main functional groups of CS was presented at 2846 cm^{-1} and 2925 cm^{-1},

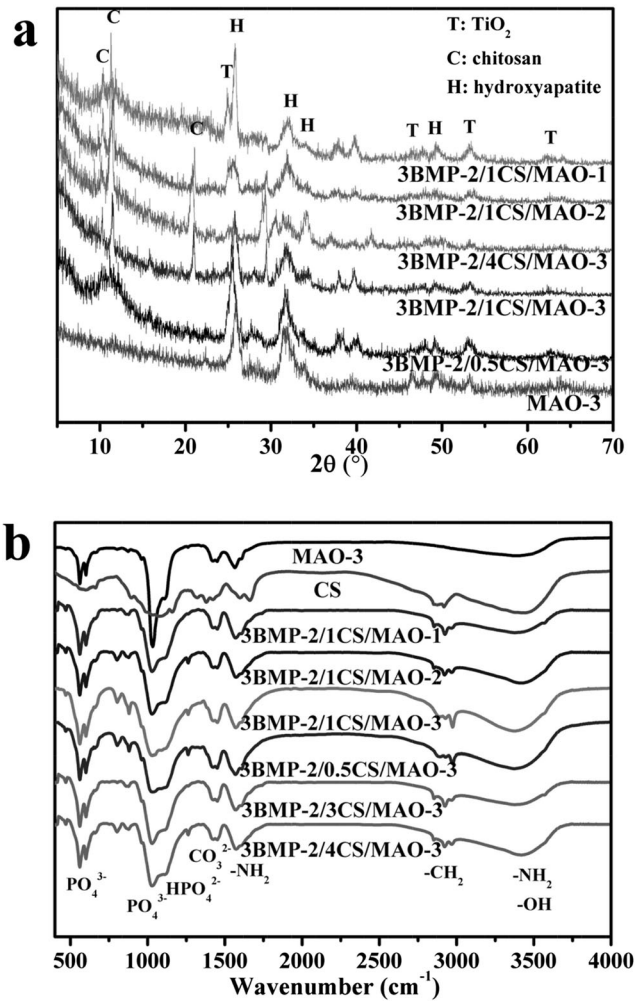

Fig. 1 XRD patterns (**a**) and FTIR spectra (**b**) of different coatings

showing the successful loading of CS on HA coatings. Besides, -NH_2 and -OH groups representing CS were also detected on BMP-2/CS/HA/TiO_2 surfaces. But there were shifts for the peaks of -NH_2 and -OH at 3441 cm^{-1} to the direction of the lower wavenumber, which is due to that -NH_2 groups of CS and -OH groups of HA formed hydrogen bonds or a complexing action occurred between -NH_2 and Ca^{2+}. Characteristic peak of -NH_2 was observed at 1573 cm^{-1} and it occurred blue shift compared with the same peak of pure CS, which was due to that N element had cross-linking effect with other elements of HA. The above results indicated that, it is not just a simple physical combination between CS and HA but chemical bonding was formed, which not only increased the bonding strength between CS and HA inside the composite coatings but between the CS contained petaling layer and porous TiO_2 layer. For different BMP-2/CS/HA/TiO_2 surfaces, there were no obvious difference for the spectral lines, suggesting that different HA thickness and CS concentration ranged from 0.5 mg/ml to 4 mg/ml do not significantly affect the chemical compositions.

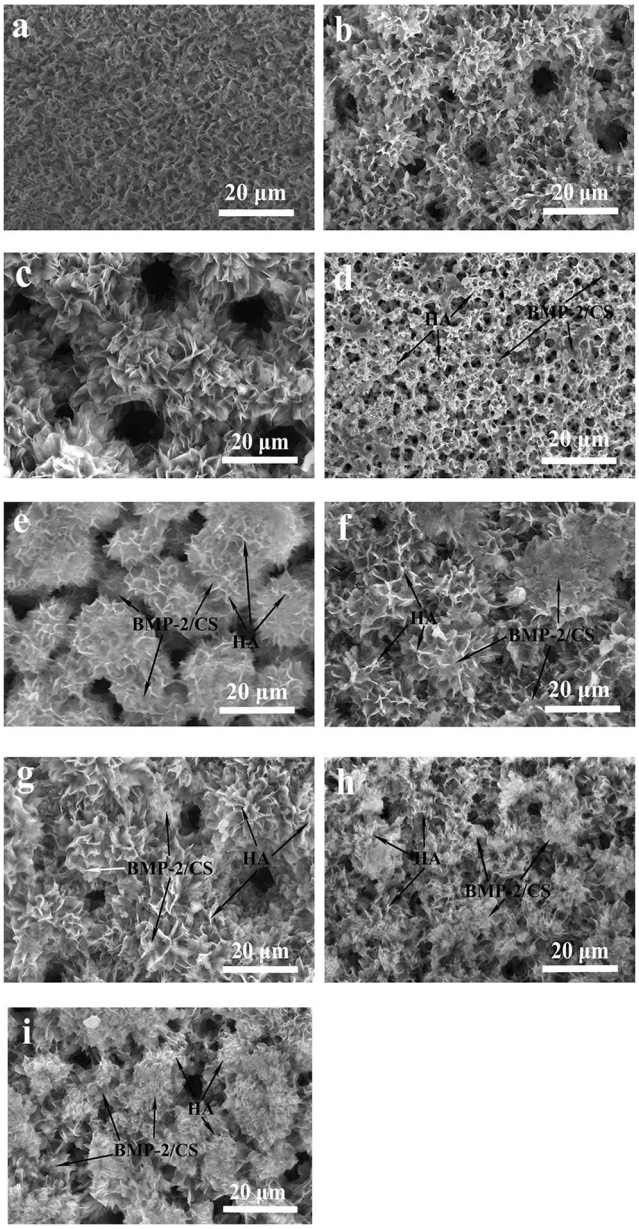

Fig. 2 surface morphology of MAO-1 (**a**), MAO-2 (**b**), MAO-3 (**c**), 3BMP-2/1CS/MAO-1 (**d**), 3BMP-2/1CS/MAO-2 (**e**), 3BMP-2/1CS/MAO-3 (**f**), 3BMP-2/0.5CS/MAO-3 (**g**), 3BMP-2/3CS/MAO-3 (**h**) and 3BMP-2/4CS/MAO-3 (**i**)

Figure 2 showed the morphology of the HA/TiO_2 and different BMP-2/CS/HA/TiO_2 coating surfaces. For HA/TiO_2 surfaces (Fig. 2a-c), petal sheets with densities of about 15–20, 25–40 and 40–50 petals/100 μm^2 were observed, and there was no obvious difference among the three surfaces excepted for the increased pore size. The formation process of the petals have been described in our previous work (Wang et al. 2018; Liu et al. 2016). In this work, the petal sheets were 4–5 μm in length, 2–3.5 μm in width, and the average spaces between petal sheets were about 1.5–3 μm. The micro pores on HA/TiO_2 surface were the results of electric breakdown, which has been reported to facilitate the growth and proliferation of cells on the material surface (Budiraharjo et al. 2012). After loading BMP-2/CS on HA/TiO_2 surface, BMP-2/CS leaked into the gaps of the petals and the oxide layer, however the surface still retained the original porous and petaling topography, seen in Fig. 2d-i (The BMP-2/CS and HA were respectively pointed out with black arrows). It can be seen that there was no obvious difference among the BMP-2/CS/HA surfaces treated by MAO with different parameters (Fig. 2d-f), while the BMP-2/CS concentration has obvious effect on surface structure (Fig. 2g-i). With the increase of BMP-2/CS concentration, more BMP-2/CS was observed on original surface, but the HA petals were still exposed outside in different degrees.

Figure 3a-c illustrated that after MAO treatment for different parameters, HA coatings were about 12, 26 and 43 μm in thickness and vertically oriented and randomly distributed on the multi-pore TiO_2 layers with thicknesses of 6, 14 and 19 μm. It was clear that the HA/TiO_2 layers had a relatively loose structure and there was a certain porosity in it, while after loading BMP-2/CS, it leaked into the gaps and the entire layer became tight and the boundaries between HA and TiO_2 layers fade away, which can promote the deformation resistance of the composite coatings and increase the adhesion strength between the HA petals and porous layers. Figure 3d-i showed that the BMP-2/CS was mixed with HA coatings without obvious stratification. The thicker the petal layer, the more BMP-2/CS leaked into it. From the cross-section images, it can also be seen that, the larger the CS concentration, the smaller the porosity of the BMP-2/CS/HA layers. The layers became denser, which was due to that more CS leaked into the petaling layers. Figure 3j showed the results of weighting method, and it can be seen that with the increase of the thickness of HA layer and CS concentration, the loaded CS amount was increased, consisting with the cross-section morphologies.

The results of surface roughness and hydrophilicity of different coatings were shown in Fig. 4. Surface roughness of BMP-2/CS/HA/TiO_2 was smaller than that of HA/TiO_2, and with the increase of CS concentration, surface roughness decreased gradually. However, there was a little increase in the roughness of BMP-2/CS/HA/TiO_2 surfaces treated by MAO with different parameters, which may be due to the increased surface roughness of HA/TiO_2 (not shown here). For BMP-2/CS/HA/TiO_2 surfaces with different CS concentration, as there were still many pores and petals not covered by CS, and there were large amount and degree of fluctuations, the surfaces still kept a high degree of roughness. Hydrophilicity is an important factor that can influence the biological properties of implant materials. In general, good hydrophilicity could facilitate a surface to adsorb serum proteins, which is also influenced by the roughness and composition of the surface. It could be observed that the HA/TiO_2 surfaces

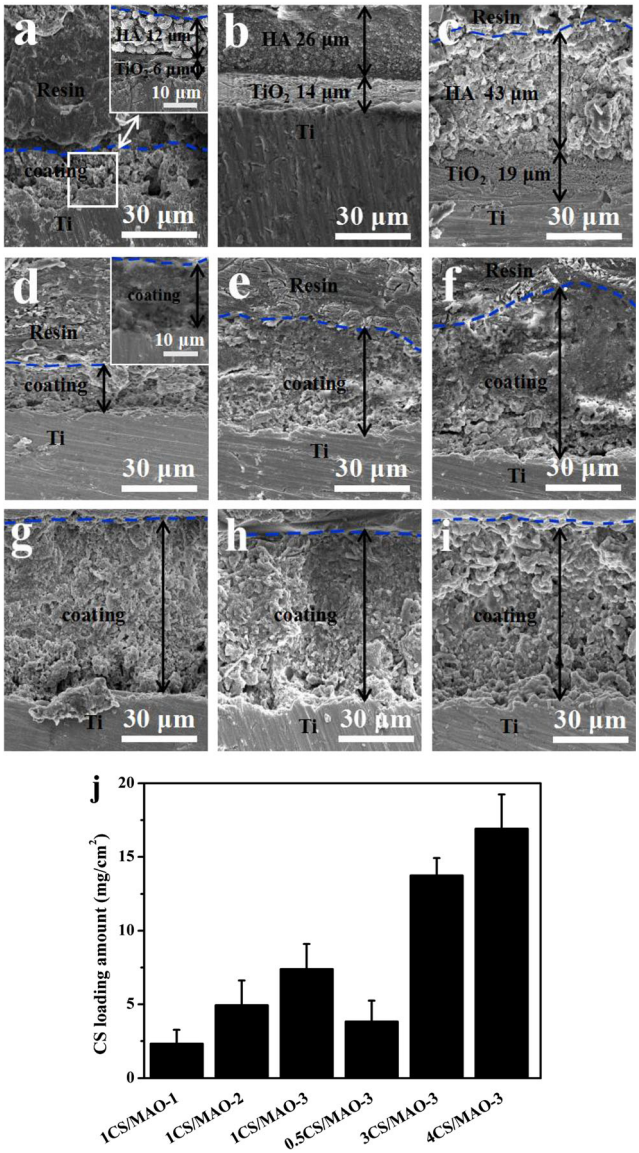

Fig. 3 Cross-sections of MAO-1 (**a**), MAO-2 (**b**), MAO-3 (**c**), 3BMP-2/1CS/MAO-1 (**d**), 3BMP-2/1CS/MAO-2 (**e**), 3BMP-2/1CS/MAO-3 (**f**), 3BMP-2/0.5CS/MAO-3 (**g**), 3BMP-2/3CS/MAO-3 (**h**), 3BMP-2/4CS/MAO-3 (**i**) and CS loading amounts of different coatings (**j**)

respectively showed water contact angles of about 21°, 15° and 0° (Fig. S1). After loading CS on surfaces, the contact angles increased to an extent, which may be due to the decrease of surface roughness that weakened the spreading of water drops on surfaces, according to Wenzel model formula (Wolansky and Marmur 1999). Surfaces with the different thickness of BMP-2/CS/HA had similar water contact angles of about 21.5°-24°. However, contact angles increased from about 18° to 34° for surfaces loading CS with concentration of 0.5–4 mg/ml, indicating the gradually decreased hydrophilicity. But all the contact angles of samples mentioned above were < 40°, suggesting good hydrophilicity. The good hydrophilicity of BMP-2/CS/HA/TiO_2 surfaces is due to that high surface roughness was maintained and CS itself is a good

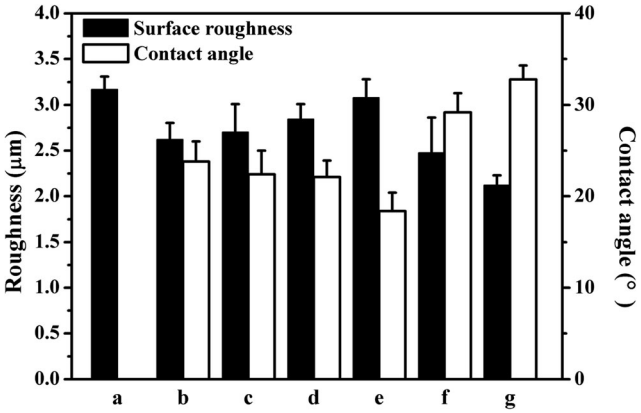

Fig. 4 The results of surface roughness and contact angles of MAO-3 (**a**), 3BMP-2/1CS/MAO-1 (**b**), 3BMP-2/1CS/MAO-2 (**c**), 3BMP-2/1CS/MAO-3 (**d**), 3BMP-2/0.5CS/MAO-3 (**e**), 3BMP-2/3CS/MAO-3 (**f**) and 3BMP-2/4CS/MAO-3 (**g**)

hydrophilic material which has many hydrophilic groups such as -OH, $-NH_2$ and NH_3^+.

3.2 Bonding strength between the composite coatings

The adhesive forces of the BMP-2/CS/HA coatings on Ti surfaces were evaluated by scratch tests and SEM observation, and the results were shown in Fig. 5. Figure 5a, c and e showed the scratch testing curves, and Fig. 5b, d and f showed the morphology of the scratches. The morphology and high magnification images indicated the trace that diamond indenter moved over through the composite layers. As the acoustic and friction signals fluctuate, it is determined to be the location of the critical load. First, the load and friction were low when the diamond indenter just touched and moved through BMP-2/CS/HA layers, therefore the acoustic signals were steady, but this process was significantly longer on the thicker layers than that on the thinner ones. During the process that diamond indenter moved on the petal layers, the coatings became dense, thinner and deformed gradually. When the load was increased, at where the scratch trace reached 0.8, 1.9 and 2.9 mm approximately, the petals layer was peeled away from the porous layer and meanwhile obvious changes in the friction and acoustic signals appeared. At this moment, the critical loads followed by the bonding strengths between the petal layers and porous layers were clear. As shown in Fig. 5a, c and e, the bonding strength were recorded as about 16, 24 and 29.7 N respectively, indicating that the resistance of BMP-2/CS/HA composite coatings to external friction and the bonding strength between the BMP-2/CS/HA and TiO_2 layers were

Fig. 5 Nick curves, the scratch' s microscopy and magnification of ▶ 3BMP-2/1CS/MAO-1 (**a, b**), 3BMP-2/1CS/MAO-2 (**c, d**) and 3BMP-2/1CS/MAO-3 (**e, f**) marked with A, B, C, D

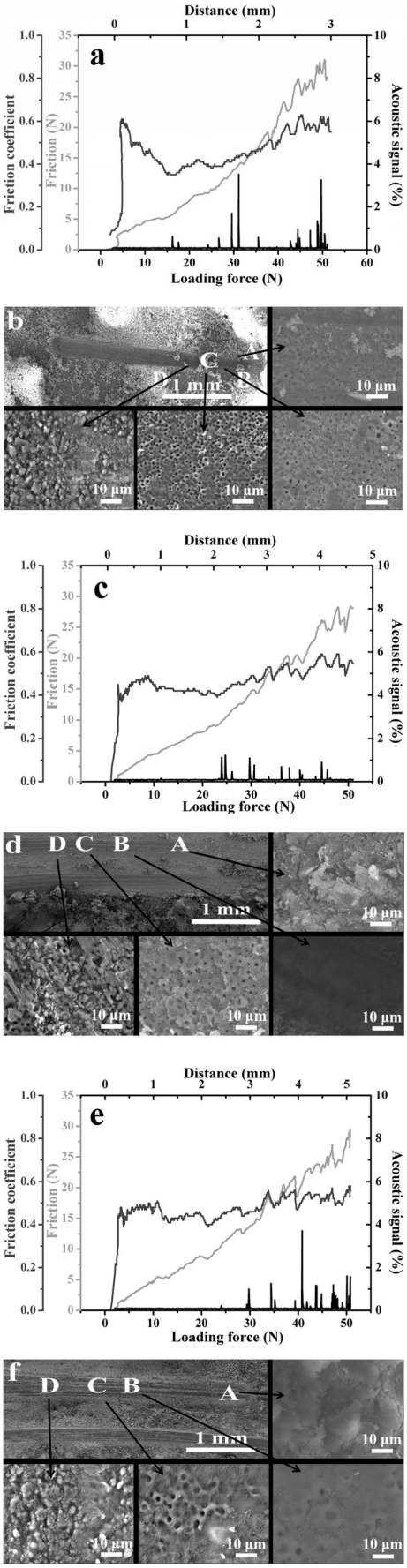

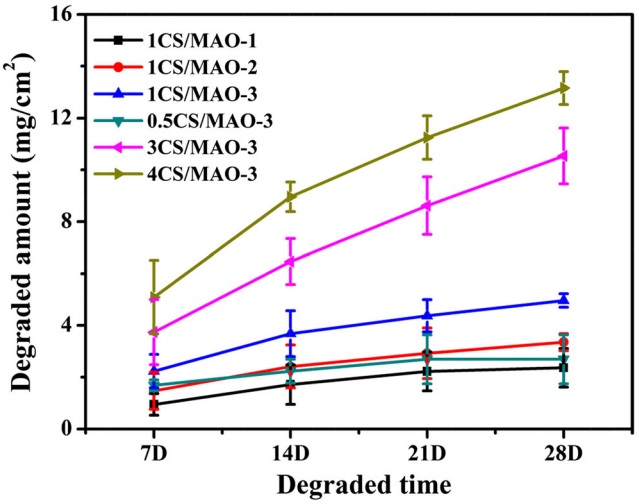

Fig. 6 Degradation amount of CS of the sample groups degraded for different days

both improved, which was due to the increased thickness of BMP-2/CS/HA layers that improved the resistance to deformation. The bonding strength could directly affect the stability

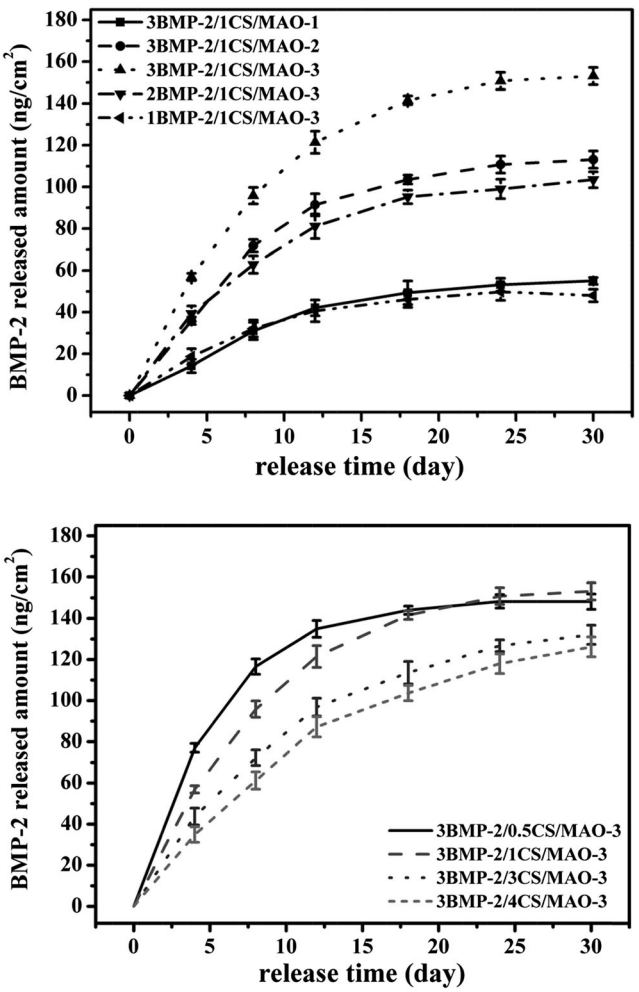

Fig. 7 BMP-2 released curves of different coatings

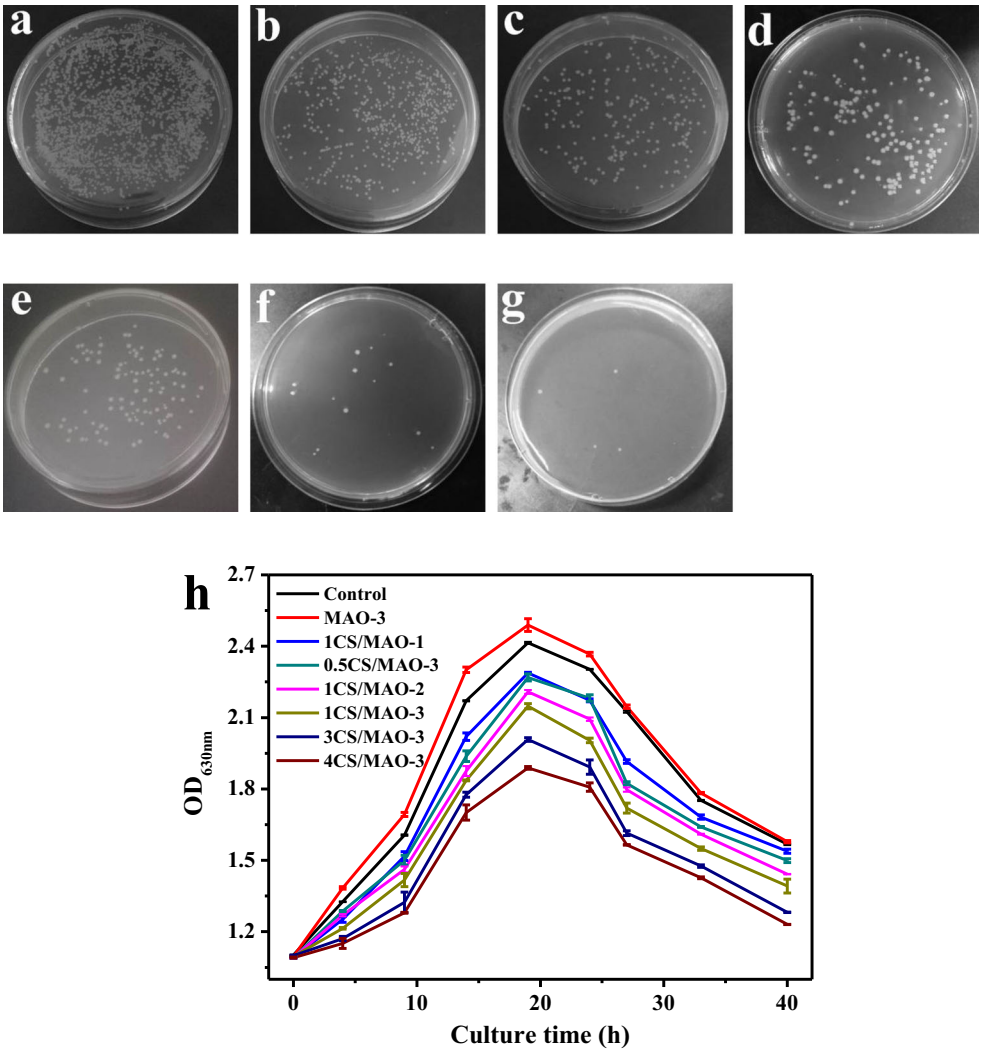

Fig. 8 Colony count of MAO-3 (**a**), 1CS/MAO-1 (**b**), 0.5CS/MAO-3 (**c**), 1CS/MAO-2 (**d**), 1CS/MAO-3 (**e**), 3CS/MAO-3 (**f**), 4CS/MAO-3 (**g**) after culturing for 24 h, and the results of optical technique of different samples within 40 h culture (**h**)

of the implant material when applied in organisms. If the composite coatings were peeled off from surfaces, the important roles of BMP-2, CS and HA to enhance biological and antibacterial properties would disappear.

3.3 Degradation of the CS containing composite coatings

Figure 6 showed the degraded CS amount of different CS/HA/TiO_2 coatings after immersion in 0.025 mg/ml PBS-lysozyme solution for different days. It can be seen that, the larger the CS concentration, the thicker the composite layers, the larger degradation rate and remanent CS amount on coating surfaces. However, with the prolonging of the degradation time, the degradation rate became slowly. In general, there are 4 steps for the degradation of polymers: (1) swelling and hydration of the polymer; (2) breakage of the ester bonds; (3) diffusion of the soluble degradation products; (4) disappearance of the polymer material chips. From the images of CS/HA/TiO_2 coatings after degradation for 6 days (Fig. S2), it can be seen that the CS amount in petal gaps decreased for all coatings and the exposed area of HA petals increased, resulting in the increase of surface roughness. And, the larger the CS concentration, the larger the residual CS on surface. CS can endow the coating with good antibacterial property, while the increase of exposed HA petals and surface roughness could induce the development of excellent biological property, but the composite coating will lose the antibacterial effect when CS degradation is completed.

3.4 *In vitro* BMP-2 release study

The release rates of BMP-2 from different BMP-2/CS/HA/TiO_2 coatings were investigated and compared, as shown in Fig. 7. BMP-2 release behavior of all BMP-2/CS/HA/TiO_2 coatings exhibited the sustained release with a biphasic release

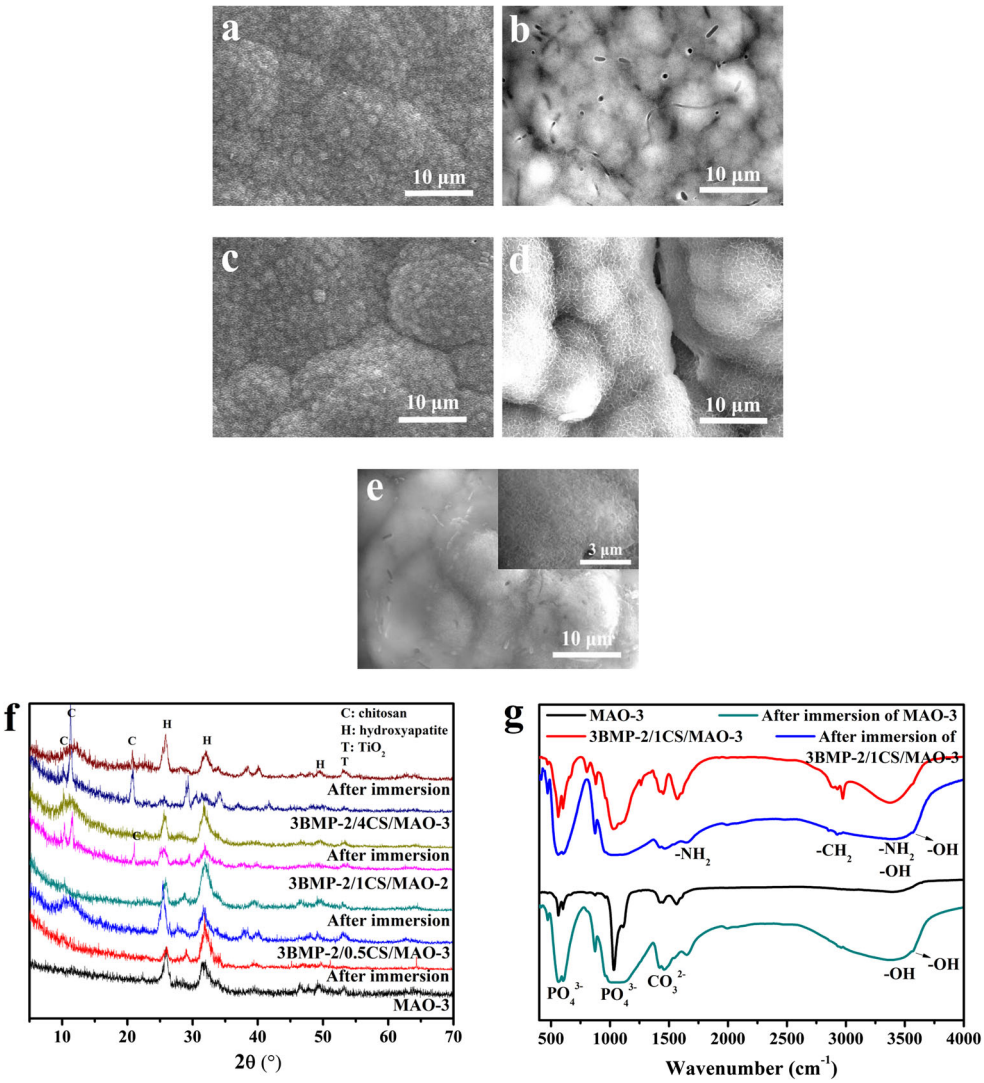

Fig. 9 SEM images of MAO-3 (**a**), 3BMP-2/1CS/MAO-1 (**b**), 3BMP-2/1CS/MAO-3 (**c**), 3BMP-2/3CS/MAO-3 (**d**), 3BMP-2/4CS/MAO-3 (**e**), XRD spectra (**f**) and FTIR spectra (**g**) of different specimens after immersed in SBF for 12 days

pattern, characterized by a fast release rate in the first week, and then followed by a slow release rate in the next 3 weeks. CS is a polymer material that can form covalent bond with BMP-2 (Hsieh et al. 2017), so that BMP-2 can only be released gradually from the composite layer with CS degradation. It is obvious that the thicker the BMP-2/CS/HA layer, the larger loading and releasing amount of the BMP-2, and the longer release period can be maintained. Besides, the loading and releasing amounts of BMP-2 can also be controlled by the BMP-2 concentration. For BMP-2/CS/HA coatings with different CS concentrations, BMP-2 release amount from the coatings gradually decreased and the release time was prolonged, meaning better BMP-2 release behavior. What worth noting is that although the degraded CS amount increased with the increase of CS concentration, the released BMP-2 amount decreased. The inconsistency may be due to the different BMP-2 concentration in CS. When the HA/TiO_2 samples were immersed in BMP-2/CS solutions, the BMP-2/CS leaked into HA petal gaps and then dried with a certain shrinkage of the volume. The lower the CS concentration, the more volume contraction of the fluid BMP-2/CS inside the petaling layer after drying, which led to higher BMP-2 density

Table 2 EDS results of different specimens before and after immersion in SBF solution (At. %)

Sample	Ca	P	C	N	Ti	O
MAO-3	21.72	14.21	4.86	0	0.05	59.16
MAO-3/12 days	27.92	16.16	5.34	0	0	50.58
BMP-2/1CS/MAO-1	15.97	10.01	7.74	3.6	0.97	61.72
BMP-2/1CS/MAO-1/12 days	19.64	12.24	5.47	1.28	0.49	60.88
BMP-2/1CS/MAO-3	20.10	11.24	9.69	1.28	0.13	57.15
BMP-2/1CS/MAO-3/12 days	23.56	14.05	5.80	0.28	0	54.30
BMP-2/4CS/MAO-3	17.06	11.90	12.75	1.98	0.04	56.26
BMP-2/4CS/MAO-3/12 days	20.77	12.79	7.90	3.24	0.03	55.27

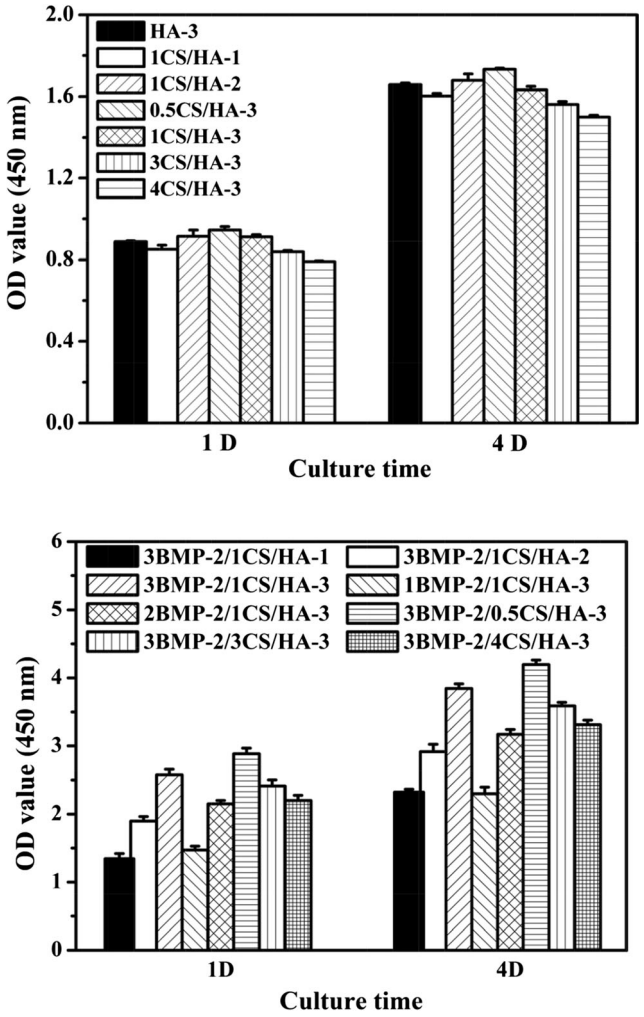

Fig. 10 CCK-8 results of different samples after co-cultured with MC3T3-E1 cells for 1 and 4 days

distributed in CS and easier release of the BMP-2 from the composite coatings.

3.5 Antibacterial activity evaluation

The antibacterial effect was evaluated by bacterial counting method and optical technique, as shown in Fig. 8. It can be seen that the percent reduction of *E. coli* for 1CS/MAO-1, 1CS/MAO-2 and 1CS/MAO-3 were approximately 70%, 85% and 95%, suggesting the improved antibacterial activity, which was because of the increased loading amount of CS. In contrast, *E. coli* cells multiplied vigorously on HA/TiO_2 coatings. In addition, the percent reduction of *E. coli* for 0.5CS/MAO-3, 3CS/MAO-3 and 4CS/MAO-3 were approximately 90%, 99% and 100% after incubation for 24 h, indicating that the antibacterial activity of CS/HA/TiO_2 can be enhanced by increasing the concentration of CS solution. This is also because of the increased loading amount of CS. It has been reported that the antibacterial mechanism of CS is due to the positive charge on CS surface, which was got by dissolving in an acid solution. The positive ions can easily adsorb the negatively charged *E. coli*, and then form a dense polymer membrane on the surface of cells, preventing the transport of nutrients to cells and the discharge of physiological metabolic wastes, causing the metabolic disorders of bacteria and affecting the growth and reproduction of bacteria (Mohamed et al. 2017; Liu et al. 2015; Liu et al. 2007). Moreover, protonated amino groups can also lead to disordered distribution of negative charges on cell membranes and cell walls, which makes it difficult for bacteria to form cell walls when they grow and then reduce the bacterial proliferation rate. The antibacterial effect of CS/HA/TiO_2 coatings was also confirmed by the optical technique. The absorbance value of the vertical axis represented the number of bacterial colonies. It showed that the absorbance value of HA/TiO_2 coating (MAO-3) was the highest, meaning no antibacterial activity. As CS was introduced to the surface, the absorbance value decreased, indicating that the antibacterial ability was endowed. With the increased thickness of the CS/HA layer and the concentration of CS solution, the absorbance value of CS/HA/TiO_2 coatings decreased, meaning gradually improved antibacterial ability.

3.6 Bioactivity evaluation

Figure 9a-e showed the surface morphology of HA/TiO_2 and BMP-2/CS/HA/TiO_2 coatings after immersion in 1.5 SBF for 12 days. It can be seen that after immersion, new substances grew entirely on all surfaces and there was no obvious difference among the surfaces in Fig. 9a-e, which were proved to be bone-like apatite (HA) seen in Fig. 9f. This is because the BMP-2/CS/HA/TiO_2 surfaces still remain large surface roughness and the HA area exposed outside, and they were further enlarged with the degradation of CS during immersion period. HA has been well known to have good bioactivity, and surfaces with large roughness have large specific surface area, which both benefit the deposition of Ca^{2+}, OH^-, PO_4^{3-} and HPO_4^{2-} groups to form apatite on surface. In addition, the energy in depression of rough surface is large, which can reduce the increment of surface energy caused by the formation of new phase (HA). The peak of CS in XRD pattern became weak and widen, suggesting a degradation occurred during immersion period. Figure 9g showed FTIR spectra of HA-3 and BMP-2/1CS/HA-3 before and after immersion. It can be seen that, the strength of peaks at 558, 602 and 1032 cm^{-1} increased after immersion, indicating that the content of PO_4^{3-} groups on surface increased and HA was formed

Fig. 11 Cells morphology on MAO-3 (**a**), 1CS/MAO-1 (**b**), 1CS/MAO-2 (**c**), 1CS/MAO-3 (**d**), 0.5CS/MAO-3 (**e**), 3CS/MAO-3 (**f**), 4CS/MAO-3 (**g**), 3BMP-2/1CS/MAO-1 (**h**), 3BMP-2/1CS/MAO-2 (**i**), 3BMP-2/1CS/MAO-3 (**j**), 2BMP-2/1CS/MAO-3 (**k**), 1BMP-2/1CS/MAO-3 (**l**) and 3BMP-2/4CS/MAO-3 (**m**) cultured for 1 day

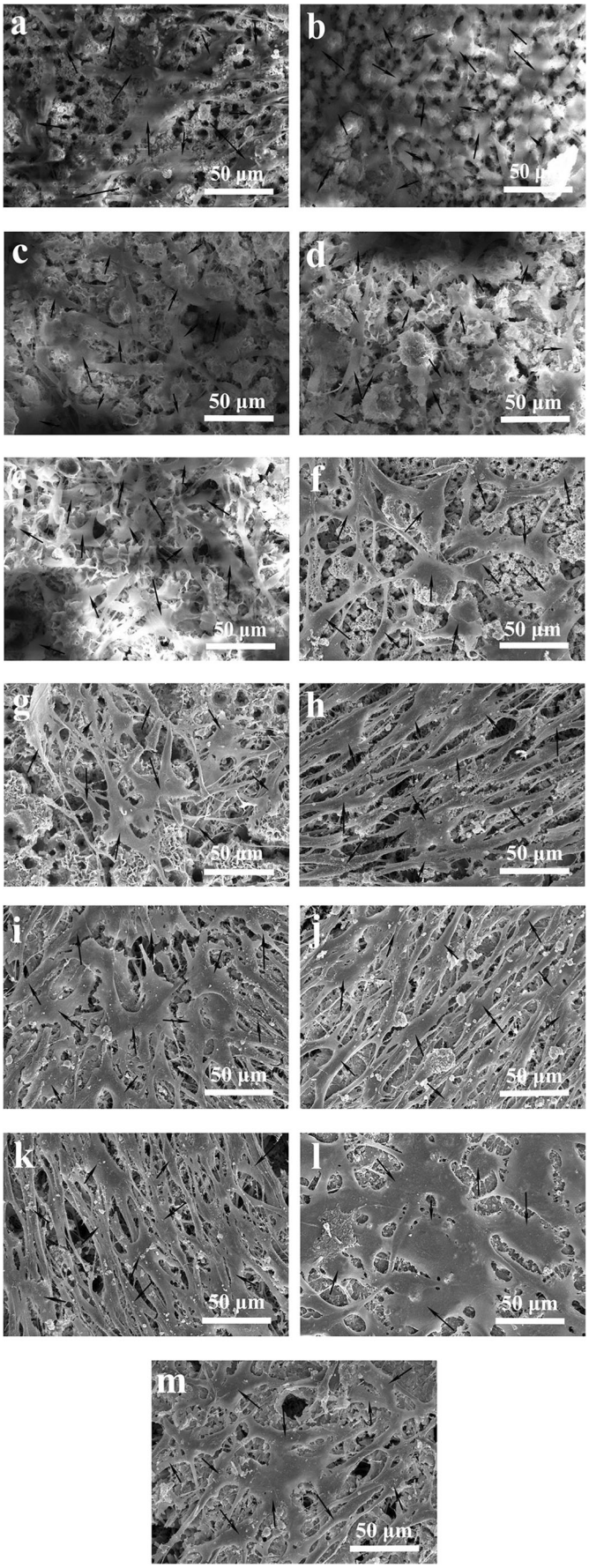
a
50 μm
b
50 μm
c
50 μm
d
50 μm
e
50 μm
f
50 μm
g
50 μm
h
50 μm
i
50 μm
j
50 μm
k
50 μm
l
50 μm
m
50 μm

on BMP-2/CS/HA surface. However, the composite absorption peak of hydroxyl and amino at 3390 cm^{-1} and the amino peak at 1573 cm^{-1} became widened and weakened, and the peak moved towards high wave number direction, indicating that CS degraded during immersion period and the reaction with HA became weakened. Besides, the number of CH bond decreased, also suggesting the degradation of CS in SBF solution. The formed HA distributed on the whole surfaces revealed that the CS film is also conducive to apatite formation. It has been widely reported that a large number of -OH and -$CONH_2$ groups in CS have a strong interaction with Ca^{2+} (Zhang et al. 2013), thus effectively promote the deposition of apatite in SBF. Moreover, the protonated -NH_2 in CS can also induce PO_4^{3-} depositing on the surface and consequently locate Ca^{2+}, leading to the formation of HA crystal nucleus on CS film (Bodhak et al. 2009; Baskar et al. 2011). Table 2 showed the element composition of the different coatings. It can be seen that after soaking in 1.5 SBF for 12 days, the content of Ca and P of the surfaces increased significantly, and the Ca/P ratio is 1.73, 1.60, 1.68 and 1.62 respectively, close to 1.67, confirming that the new substances formed on coating surfaces were HA and all the surfaces have good bioactivity, which was consistent with the surface morphology of Fig. 9a-e.

3.7 Biocompatibility evaluation

Cell proliferation on the specimens was assessed by CCK-8, and the results were shown in Fig. 10. The high OD value means a higher cell proliferation on specimen surface. During the experimental period, the cell number on all surfaces increased. We can see that the cells proliferated much faster on the BMP-2 immobilized coating surfaces than on HA/TiO_2 and CS/HA/TiO_2 surfaces, and the OD value was almost directly related to the released BMP-2 amount, suggesting the strong effect of BMP-2 on cells proliferation. And it can be controlled by the thickness of BMP-2/CS/HA layers and BMP-2 concentration. Besides, the BMP-2/CS/HA/TiO_2 surfaces still maintains large surface roughness and exposed HA area, which are both important factors that can also facilitate the growth and proliferation of the cells on surface (Wang et al. 2017; Budiraharjo et al. 2012; Cai et al. 2011). What's more, evidence mounted supporting the idea that hydroxyl groups, which were existed in both HA and CS, were particularly stimulatory to cell adhesion and proliferation. For HA/TiO_2 and CS/HA/TiO_2 coatings, the cells proliferated faster on the HA/TiO_2 surfaces than those on most CS/HA/TiO_2 surfaces, and the cell number on CS/HA/TiO_2 coatings decreased with the increase of CS concentration. However, with the increase of CS concentration, the surfaces still kept high cells proliferation rate, which was due to the increased surface roughness and exposed HA after the degradation of CS. Besides, it has been reported that surface with water angle of 20°-40° is the most beneficial for cells adhesion, spreading and proliferation on surface (Tang et al. 2014), which is a favourable factor to explain the good biocompatibility of CS/HA.

Figure 11 showed the morphology of MC3T3-E1 cells cultured on different surfaces for 1 day (The cells were pointed out with black arrows). It can be seen that MC3T3-E1 cells can grow well on all surfaces, and cells showed a typical polygonal osteoblastic shape and there were many finger-like protrusions and filopodia stretching out from the cell bodies. Obviously, more cells adhered on BMP-2 immobilized surfaces and cells grew larger and connected each other with more pseudopodia, and there was no difference among the surfaces immobilized with different BMP-2, indicating the strong inductive effect of BMP-2 on cells adhesion and spreading on surfaces. For HA/TiO_2 and CS/HA/TiO_2 surfaces, no significant difference in cell morphology can be observed. Cells on these surfaces grew well with a lot of pseudopodiums stretching from cells bodies, confirming excellent biocompatibility.

Based on the above results, it was known that, petal-like HA layers with different thickness were prepared on Ti surfaces by increasing the applied current and oxide time, and the many micro-gaps in petaling HA coatings can be convenient carriers for drugs and biomaterials to endow the surface with comprehensive or specific performance. It was the first time to find that the good antibacterial activity against *E. coli* can be achieved by increasing the loading amount of CS on surface, and the increased CS amount can be obtained through increasing the thickness of HA layer and the CS concentration. In this work, 3BMP-2/4CS/HA-3 had the optimal performance, because the maximum amount of CS and BMP-2 was introduced to the surface of this sample and it has the best BMP-2 release behavior, which made the sample have the best antibacterial and biological properties when compared with the other samples, and the improved properties can maintain for a longer time than the other samples. In addition, the excellent biocompatibility and bioactivity may also be related to its high surface roughness and suitable hydrophilicity.

4 Conclusion

In this work, CS/HA/TiO_2 and BMP-2/CS/HA/TiO_2 coatings were prepared on Ti surfaces. The micro-structure, CS loading and releasing amount, BMP-2 release behavior, antibacterial activity and biological properties can be improved through the proper control of the thickness of HA layer, BMP-2 and CS concentrations. The thicker the HA coating, the larger the loading and releasing amount of BMP-2 and CS, which also improved bonding strength between the BMP-2/CS/HA and porous TiO_2 layers, improved the release behavior of BMP-2, antibacterial and biological property of the surface coatings. In

addition, with the increase of CS concentration, the CS loading and degrading amounts, antibacterial activity and BMP-2 release behavior were also enhanced, and meanwhile maintaining the good biological properties. BMP-2 can significantly improve the biocompatibility of all CS/HA/TiO_2 surfaces, and its loading amount and release behavior can be controlled by the thickness of HA layer and BMP-2 concentration.

Acknowledgements The authors gratefully acknowledge the support by the National Natural Science Foundation of China (Project No.51201056), Technology Foundation for returned overseas Chinese scholars (No.C2015003038) and Natural Science Foundation of Hebei Province of China (Project No. E2013202021, No. E2017202032).

Compliance with ethical standards

Conflict of interest The authors have declared that no COI exists.

References

A. Arifin, A.B. Sulong, N. Muhamad, J. Syarif, M.I. Ramli, Material processing of hydroxyapatite and titanium alloy (HA/Ti) composite as implant materials using powder metallurgy: A review. Mater. Des. **55**, 165–175 (2014)

D. Baskar, R. Balu, T.S. Kumar, Mineralization of pristine chitosan film through biomimetic process. Int. J. Biol. Macromol. **49**, 385–389 (2011)

S. Bodhak, S. Bose, A. Bandyopadhyay, Role of surface charge and wettability on early stage mineralization and bone cell-materials interactions of polarized hydroxyapatite. Acta Biomater. **5**, 2178–2188 (2009)

R. Budiraharjo, K.G. Neoh, E.T. Kang, Hydroxyapatite-coated carboxymethyl chitosan scaffolds for promoting osteoblast and stem cell differentiation. J. Colloid Interface Sci. **366**, 224–232 (2012)

L. Cai, A.S. Guinn, S. Wang, Exposed hydroxyapatite particles on the surface of photo-crosslinked nanocomposites for promoting MC3T3 cell proliferation and differentiation. Acta Biomater. **7**, 2185–2199 (2011)

L. Han, M.H. Wang, H.L. Sun, P.F. Li, K.F. Wang, F.Z. Ren, X. Lu, Porous titanium scaffolds with self-assembled micro/nano hierarchical structure for dual functions of bone regeneration and anti-infection. J. Biomed. Mater. Res. A **105**(1–14), 3482 (2017)

X.N. He, Y. Liu, X. Yuan, L. Lu, Enhanced healing of rat Calvarial defects with MSCs loaded on BMP-2 releasing chitosan/alginate/hydroxyapatite scaffolds. PLoS One **9**, e104061 (2014)

M. He, B.Q. Han, Z.W. Jiang, Y. Yang, Y.F. Peng, W.S. Liu, Synthesis of a chitosan-based photo-sensitive hydrogel and its biocompatibility and biodegradability. Carbohydr. Polym. **166**, 228–235 (2017)

M.Y. Hsieh, L.Y. Yang, J.M. Chem, W.F. Lee, Y.Y. Huang, Treatment of the avascular necrosis with a novel biodegradable thermosensitive box hydrogel carrying BMP-2. Sci. Adv. Mater. **9**, 815–823 (2017)

R.X. Li, C. Xu, Y.J. Liu, H. Li, C.H. Shi, W.H. Su, W.N. An, Y.H. Yuan, X.L. Qin, Y.Q. Xu, X.Z. Zhang, H. Li, Degradation behavior and compatibility of micro, nanoHA/chitosan scaffolds with interconnected spherical macropores. Int. J. Biol. Macromol. **103**, 385–394 (2017)

X.F. Liu, L. Song, L. Li, S.Y. Li, K.D. Yao, Antibacterial effects of chitosan and its water-soluble derivatives on E. coli, plasmids DNA, and mRNA. J. Appl. Polym. Sci. **103**, 3521–3528 (2007)

H.H. Liu, H.J. Peng, Y. Wu, C. Zhang, Y.Z. Cai, G.W. Xu, Q. Li, X. Chen, J.F. Ji, Y.Z. Zhang, W.H. Ouyang, The promotion of bone regeneration by nanofibrous hydroxyapatite/chitosan scaffolds by effects on integrin-BMP/Smad signaling pathway in BMSCs. Biomaterials. **34**, 4404–4417 (2013)

X.L. Liu, W.S. Xia, Q.X. Jiang, Y.S. Xu, P.P. Yu, Effect of kojic acid-grafted-chitosan oligosaccharides as a novel antibacterial agent on cell membrane of gram-positive and gram-negative bacteria. J. Biosci. Bioeng. **120**, 335–339 (2015)

S.M. Liu, B.E. Li, C.Y. Liang, H.S. Wang, Z.X. Qiao, Formation mechanism and adhesive strength of a hydroxyapatite/TiO_2 composite coating on a titanium surface prepared by micro-arc oxidation. Appl. Surf. Sci. **362**, 109–114 (2016)

B. Lowe, J. Venkatesan, S. Anil, M.S. Shim, S.K. Kim, Preparation and characterization of chitosan-natural nano hydroxyapatite-fucoidan nanocomposites for bone tissue engineering. Int. J. Biol. Macromol. **93**, 1479–1487 (2016)

R.R. Mohamed, M.H. Elella, M.W. Sabaa, Cytotoxicity and metal ions removal using antibacterial biodegradable hydrogels based on N-quaternized chitosan/poly (acrylic acid). Int. J. Biol. Macromol. **98**, 302–313 (2017)

Z.Y. Peng, Z.P. Li, F. Zhang, X.C. Peng, In-vitro degradation and cytotoxicity of gelatin/chitosan microspheres for drug controlled release. J. Macromol. Sci. A **51**, 646–652 (2014)

H. Sharifi, M. Aliofkhazraei, G.B. Darband, S. Shrestha, A review on adhesion strength of peo coatings by scratch test method. Surf. Rev. Lett. **1830004** (2018)

A. Skodje, S.B. Idris, Y. Sun, S. Bartaula, K. Mustafa, A. Finne-Wistrand, U.M. Wikesjö, K.N. Leknes, Biodegradable polymer scaffolds loaded with low-dose BMP-2 stimulate periodontal ligament cell differentiation. J. Biomed. Mater. Res. A **103**, 1991–1998 (2015)

T.F. Sun, K. Zhou, M. Liu, X.D. Guo, Y.Z. Qu, W. Cui, Z.W. Shao, X.L. Zhang, S.Y. Xu, Loading of BMP-2-related peptide onto three-dimensional nano-hydroxyapatite scaffolds accelerates mineralization in critical-sized cranial bone defects. J. Tissue Eng. Regen. Med. **12**, 864–877 (2018)

S. Tang, B. Tian, Y.J. Guo, Z.A. Zhu, Y.P. Guo, Chitosan/carbonated hydroxyapatite composite coatings: Fabrication, structure and biocompatibility. Surf. Coat. Technol. **251**, 210–216 (2014)

G.C. Wang, J.C. Qiu, L. Zheng, N. Ren, J.H. Li, H. Liu, J.Y. Miao, Sustained delivery of BMP-2 enhanced osteoblastic differentiation of BMSCs based on surface hydroxyapatite nanostructure in chitosan-HAp scaffold. J. Biomater. Sci. Polym. Ed. **25**, 1813–1827 (2014)

X.Y. Wang, Z.M. Qu, J.J. Li, E.L. Zhang, Comparison study on the solution-based surface biomodification of titanium: Surface characteristics and cell biocompatibility. Surf. Coat. Technol. **329**, 109–119 (2017)

X.L. Wang, B.E. Li, L.X. Zhou, J.W. Ma, X.L. Zhang, H.P. Li, C.Y. Liang, S.M. Liu, H.S. Wang, Influence of surface structures on biocompatibility of TiO_2/HA coatings prepared by MAO. Mater. Chem. Phys. **215**, 339–345 (2018)

G. Wolansky, A. Marmur, Apparent contact angles on rough surfaces: The Wenzel equation revisited. Colloids Surf., A **156**, 381–388 (1999)

C. Yu, L.Y. Cui, Y.F. Zhou, Z.Z. Han, X.B. Chen, R.C. Zeng, Y.H. Zou, S.Q. Li, F. Zhang, E.H. Han, S.K. Guan, Self-degradation of micro-arc oxidation/chitosan composite coating on mg-4Li-1Ca alloy. Surf. Coat. Technol. **344**, 1–11 (2018a)

W.Z. Yu, Y.Z. Zhang, X.M. Liu, Y.M. Xiang, Z.Y. Li, S.L. Wu, Synergistic antibacterial activity of multi components in lysozyme/chitosan/silver/hydroxyapatite hybrid coating. Mater. Des. **139**, 351–362 (2018b)

Y.P. Yun, The effect of bone morphogenic protein-2 (BMP-2) - immobilizing heparinized - chitosan scaffolds for enhanced osteoblast activity. J. Tissue Eng. Regen. Med. **10**, 122–130 (2013)

J. Zhang, C.S. Dai, J. Wei, Z.H. Wen, S.J. Zhang, L.M. Lin, Calcium phosphate/chitosan composite coating: Effect of different concentrations of Mg^{2+} in the m-SBF on its bioactivity. Appl. Surf. Sci. **280**, 256–262 (2013)

Y.G. Zhang, Y.J. Zhu, F. Chen, T.W. Sun, A novel composite scaffold comprising ultralong hydroxyapatite microtubes and chitosan: Preparation and application in drug delivery. J. Mater. Chem. B **5**, 3898–3906 (2017)

Publisher's note Springer Nature remains neutral with regard to jurisdictional claims in published maps and institutional affiliations.